NANO LETTERS

LETTER

pubs.acs.org/NanoLett

Visible Light Photocatalytic H_2-Production Activity of CuS/ZnS Porous Nanosheets Based on Photoinduced Interfacial Charge Transfer

Jun Zhang,[†] Jiaguo Yu,[*,†] Yimin Zhang,[†] Qin Li,[‡,†] and Jian Ru Gong[*,‡]

[†]State Key Laboratory of Advanced Technology for Materials Synthesis and Processing, College of Resource and Environmental Engineering, Wuhan University of Technology, Wuhan 430070, People's Republic of China

[‡]National Center for Nanoscience and Technology, 11 Zhongguancun Beiyitiao, Beijing 100190, People's Republic of China

Supporting Information

ABSTRACT: Visible light photocatalytic H_2 production through water splitting is of great importance for its potential application in converting solar energy into chemical energy. In this study, a novel visible-light-driven photocatalyst was designed based on photoinduced interfacial charge transfer (IFCT) through surface modification of ZnS porous nanosheets by CuS. CuS/ZnS porous nanosheet photocatalysts were prepared by a simple hydrothermal and cation exchange reaction between preformed $ZnS(en)_{0.5}$ nanosheets and $Cu(NO_3)_2$. Even without a Pt cocatalyst, the as-prepared CuS/ZnS porous nanosheets reach a high H_2-production rate of 4147 μmol h^{-1} g^{-1} at CuS loading content of 2 mol % and an apparent quantum efficiency of 20% at 420 nm. This high visible light photocatalytic H_2-production activity is due to the IFCT from the valence band of ZnS to CuS, which causes the reduction of partial CuS to Cu_2S and thus enhances H_2-production activity. This work not only shows a possibility for substituting low-cost CuS for noble metals in the photocatalytic H_2 production but also for the first time exhibits a facile method for enhancing H_2-production activity by photoinduced IFCT.

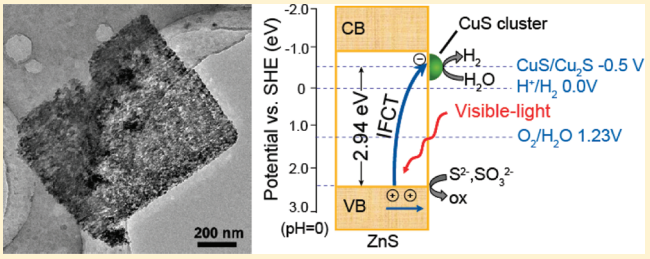

KEYWORDS: Photocatalytic hydrogen production, CuS, ZnS, porous nanosheet, interfacial charge transfer, visible light

As a potential answer to the global energy crisis and environmental pollution, the application of hydrogen energy has attracted great attention.[1] However, hydrogen is mainly produced from fossil fuels or the high-energy consumption process at present, which is not environmentally friendly and economical.[2] Since Fujishima and Honda first reported the photoelectrochemical water-splitting on a TiO_2 electrode,[3] photocatalytic water-splitting for hydrogen production has become a promising approach for clean, economical, and environmentally friendly production of hydrogen by using solar energy. Numerous active photocatalysts for splitting water have been synthesized and investigated in the past few decades,[4−8] whereas most of these photocatalysts can solely absorb the UV light, which accounts for only 4% of the total sunlight, and thus greatly restricts its practical applications. Hence, it is highly desirable to develop photocatalysts with high activities under visible light illumination.

Recently, metal sulfides have been intensively studied in photocatalysis because of their suitable bandgap and catalytic functions. In particular, ZnS is a well-known photocatalyst as a result of the rapid generation of electron−hole pairs by photoexcitation and the highly negative potentials of excited electrons, showing high activity for H_2 evolution, even without any assistance of noble metal cocatalysts.[9−11] While the bandgap of ZnS (3.66 eV) is too large for visible light response,[10] and many methods such as doping with metal ions (i.e., Ni^{2+}, Cu^{2+}, and Pb^{2+}),[12−15] preparing solid solutions and combining with various narrow bandgap semiconductors have been applied to make ZnS have visible light activity.[16,17] In recent years, sulfide solid solutions such as $Cu_xZn_{1-x}S$, $Zn_xCd_{1-x}S$, Cu−$Zn_xCd_{1-x}S$ and CuS−In_2S_3−ZnS have been proved to be an efficient visible light driven photocatalysts for H_2 production from water splitting.[13,17−26] Unfortunately, cadmium is a widespread environmental pollutant, which is toxic and harmful to human beings. Moreover, in order to achieve high crystallinity, a high-temperature heat treatment is usually needed for the preparation of these solid solutions and sometimes an expensive Pt cocatalyst is still needed for the higher quantum efficiency. In addition, the morphology of these solid solutions through solid-state reaction or coprecipitation method is usually irregular (e.g., bulk or aggregate of nanoparticles). In this case, the facile preparation of well-crystallized and low-toxic ZnS-based photocatalysts with controllable morphology and high photocatalytic activity is still a challenge.

In this work, for the first time we reported the fabrication of CuS/ZnS porous nanosheets by a simple hydrothermal and

Received: July 28, 2011
Revised: September 21, 2011
Published: October 07, 2011

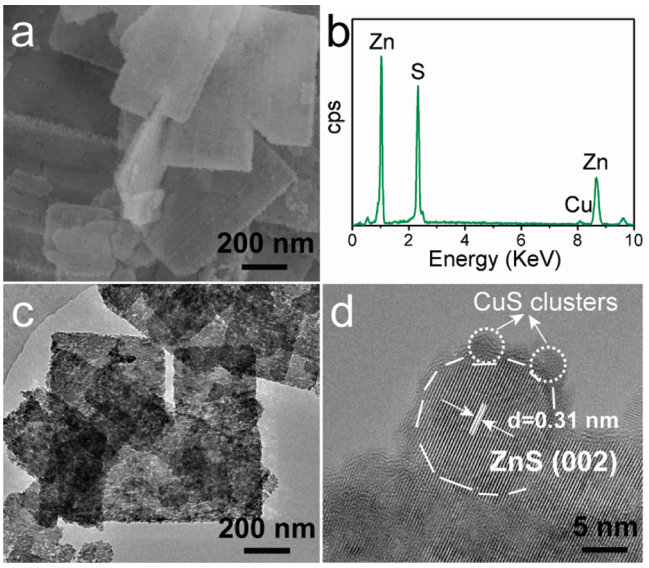

Figure 1. SEM image (a), EDX pattern (b), TEM (c), and HRTEM image (d) of sample CZ2.

cation exchange method using preformed $ZnS(en)_{0.5}$ nanosheets and $Cu(NO_3)_2$ as precursors, and their highly visible light-driven photocatalytic H_2-production activity from aqueous solutions containing Na_2S and Na_2SO_3 without Pt cocatalyst. Furthermore, the photoinduced interfacial charge transfer (IFCT) mechanism was first proposed to explain the origin for the visible light induced response and enhanced visible light H_2-production activity by loading CuS.

CuS/ZnS porous nanosheets were prepared by hydrothermal method instead of high-temperature calcinations,[27−30] that is, by cation exchange reaction using the preformed $ZnS(en)_{0.5}$ nanosheets and Cu^{2+} ions as precursors at 140 °C for 12 h. A series of samples with the nominal Cu^{2+}/Zn^{2+} molar ratio x were labeled as CZx (x = 0, 0.5, 1, 2, 3, and 5 mol %), respectively, and the Cu^{2+} concentration in these samples was measured by inductively coupled plasma atomic emission spectrometry (ICP-AES) (see details in Supporting Information). The typical SEM image (CZ2 with the highest H_2-production activity) is shown in Figure 1a. It can be seen clearly that the sheet structures are basically remained after the hydrothermal treatment of $ZnS(en)_{0.5}$ precursor, while some nanoparticles appear on the surface of these nanosheets, becoming rougher compared with the original smooth surface of $ZnS(en)_{0.5}$ nanosheets (Figure S1a in Supporting Information). The energy-dispersive X-ray (EDX) spectrum (Figure 1b) confirms that the CZ2 sample consists of zinc, copper, and sulfur elements. Also, the sample exhibits sheetlike morphology with clear porous structure in the transmission electron microscopy (TEM) image (Figure 1c). These nanosheets are composed of numerous nanoparticles with diameters ca. 20 nm and the pores are formed between these nanoparticles. From the high-resolution TEM (HRTEM) image in Figure 1d, the lattice fringes can be clearly observed, suggesting the well-defined crystal structure, and the fringe with lattice spacing of ca. 0.31 nm corresponds to the (002) plane of the hexagonal ZnS. Notably, it can be observed that some small clusters with the size of ca. 2−5 nm are deposited on the surface of ZnS particles (as indicated in Figure 1d). Associated with the EDX results (EDX confirms the presence of copper element) and

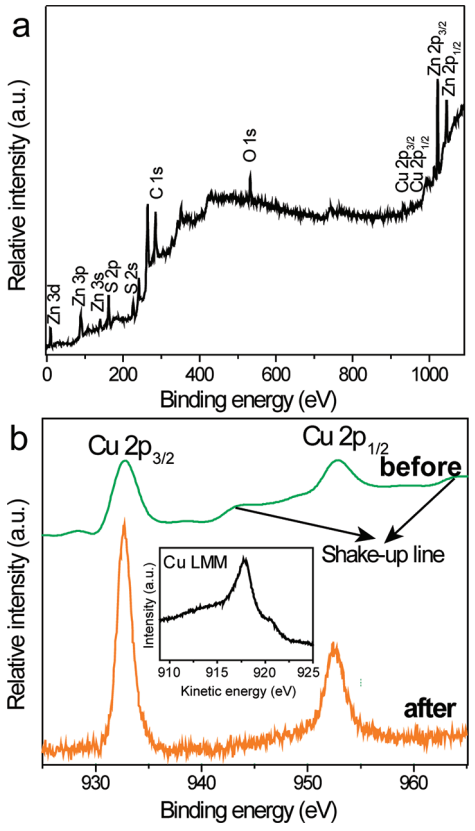

Figure 2. (a) Typical XPS survey spectrum of sample CZ2, and (b) Cu 2p region of the XPS spectra of the sample CZ2 before and after 2 h photocatalytic reaction under visible light irradiation. The inset in Figure 2b is Auger Cu LMM spectrum of sample CZ2 after photocatalytic reaction for 2 h.

discussions below, it can be concluded that these small clusters are consisted of CuS nanoparticles. The close interconnection (or heterojunction) between ZnS and CuS by cation exchange reactions is believed to favor the vectorial transfer of photogenerated electrons from ZnS to CuS, thus enhancing the charge separation and photocatalytic efficiency.[31,32] In this case a question subsequently arises, namely, how does the sheetlike porous structure form? It is proposed that during the hydrothermal treatment of $ZnS(en)_{0.5}$ precursor, the $ZnS(en)_{0.5}$ nanosheets are unstable and completely decompose to ZnS first while the sheetlike structure remains unchanged.[30] Then, ZnS nanocrystallites in situ nucleate and preferentially grow on the surface of the sheets due to the fact that the interface nucleation has the lowest activation energy of nucleation.[33] This results in the formation of the sheetlike porous structure.

The complete conversion of $ZnS(en)_{0.5}$ to ZnS under our hydrothermal experimental conditions is proved by the XRD patterns of CZx with the diffraction peaks for all samples are well indexed to ZnS wurtzite phase [JCPDS No. 36-1450, space group: P63mc (186)] as shown in Figure S2 in Supporting Information. However, CuS phase is not detected by XRD even though the molar concentration of CuS is as high as 5% (CZ5) owing to the weak crystallization and high dispersion of CuS particles deposited on the surface of ZnS nanoparticles.[34] It is worth noting that the diffraction peaks of ZnS become weaker and the widths of the peaks become slightly wider with increasing CuS content, implying a decrease in the crystallinity and the

dx.doi.org/10.1021/nl202587b |Nano Lett. 2011, 11, 4774–4779

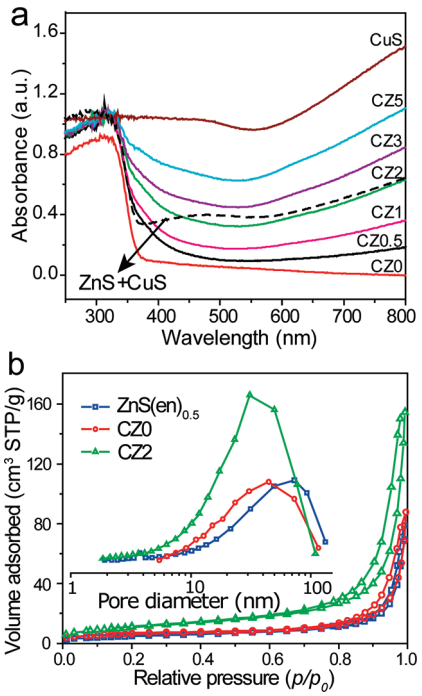

Figure 3. (a) UV−vis absorption spectra of CZ*x* samples as well as CuS and ZnS + CuS. ZnS + CuS: physical mixture of CuS and ZnS (i.e., CZ0) (the molar content of CuS is 2%). (b) Nitrogen adsorption−desorption isotherms and the corresponding pore size distribution curves of ZnS-$(en)_{0.5}$ precursor, CZ0, and CZ2.

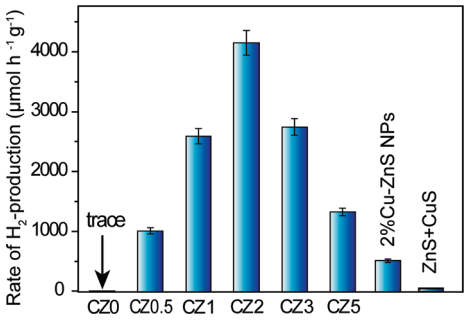

Figure 4. Comparison of the visible light photocatalytic H_2-production activity of CuS/ZnS porous nanosheets and ZnS samples under visible light ($\lambda \geq 420$ nm) with the mixed aqueous solution containing 0.35 M Na_2S and 0.25 M Na_2SO_3 as sacrificial solution; light source: 350 W xenon arc lamp.

average crystallite size. The average crystallite size of ZnS, which is determined by the broadening of the (002) diffraction peak using the Debye−Scherrer formula,[35] decreases from 19.8 to 15.7 nm with increasing CuS content from 0 to 5% as listed in Supporting Information Table S1.

To analyze the chemical composition of the prepared samples and to identify the chemical status of Cu element in the samples, X-ray photoelectron spectroscopy (XPS) analysis was carried out. Figure 2a exhibits the XPS survey spectrum of CZ2 and the peaks of Cu 2p, S 2p, Zn 2p, O 1s, and C 1s can be clearly observed. The weak peaks of O and C come from H_2O, O_2, and CO_2 adsorbed on the surface of the sample and adventitious hydrocarbon from XPS instrument itself, respectively.[36] The high-resolution XPS spectrum of Cu in the 2p region for CZ2 before the photocatalytic reaction (Figure 2b) shows the binding energies of Cu $2p_{3/2}$ and Cu $2p_{1/2}$ peaks at 932.7 and 952.8 eV, respectively, which are typical values for Cu^{2+} in CuS.[37−39] Meanwhile, two shakeup lines at 943.2 and 963.6 eV are observed, indicating the paramagnetic chemical state of Cu^{2+}.[38] Furthermore, symmetrical shapes of the two Cu 2p XPS peaks also imply the presence of pure CuS. However, after photocatalytic reaction for 2 h, the XPS spectrum of CZ2 exhibits a significant change. Two shakeup lines almost disappear and the binding energies of Cu $2p_{3/2}$ and Cu $2p_{1/2}$ slightly left-shift to 932.5 and 952.4 eV, respectively, indicating the presence of either Cu^0 or Cu^{1+}. However, associate with the Auger Cu LMM spectrum of sample CZ2 after photocatalytic reaction for 2 h (inset in Figure 2b), the Cu LMM line position is found at around 917.6 eV, which suggests that Cu^0 does not seem to be present since its characteristic feature (Cu LMM at 918.7 eV) is not detected.[40] From this brief analysis, it is realistic to assume that after photocatalytic reaction for 2 h, a small amount of Cu^{2+} in CuS is reduced to Cu_2S. These results also confirm the electron transfer from the CB of ZnS to CuS and the partial reduction of CuS to Cu_2S.

Figure 3a shows the UV−vis diffuse reflection spectra of the samples CZ*x* (x = 0, 0.5, 1, 2, 3, and 5). A significant increase in the absorption at wavelengths shorter than 365 nm can be assigned to the intrinsic bandgap absorption of ZnS,[41] and the bandgap energy is estimated to be 3.35 eV according to the Kubelka−Munk method.[42] As for CZ*x* samples, with increasing the content of CuS an enhanced absorption in the visible light region (at wavelength over 400 nm) is clearly observed. This enhancement is ascribed to increasing the content of CuS, which has an obvious absorption in the range of 300−800 nm (as shown in the spectrum of the pure CuS).[13,43] The absorption at 700−800 nm can be assigned to the d−d transition of Cu(II).[44−47] In addition, there is no shift in the absorption edge of the CZ*x* samples in comparison to that of pure ZnS (sample CZ0), further implying that CuS is only deposited on the ZnS surface instead of incorporating to the lattice of ZnS. Furthermore, in comparison with the absorption spectrum of the physical mixture of CuS and ZnS (sample ZnS + CuS), an absorption shoulder from ∼350 to 450 nm can be distinctly observed for sample CZ2. By analogy to the reported IFCT from the VB of TiO_2 to Cu(II),[44−47] the absorption shoulder from ∼350 to 450 nm can be ascribed to the direct IFCT from the VB of ZnS to CuS. This photoinduced charge transfer has also been confirmed by the above XPS results that electrons are photoexcited from VB of ZnS directly to CuS and then reduce partial CuS to Cu_2S. In contrast, sample ZnS+CuS shows negligible visible light H_2-production activity (see Figure 4 as discussed later) due to the loose contact between ZnS and CuS. This fact associated with the UV−vis and TEM results indicates that the intimate contact between CuS and ZnS via the cation exchange reaction is crucial for the interelectron transfer between the two components, which result in the possibility for the direct IFCT from the VB of ZnS to CuS and the visible light activity.

It is well-known that heterogeneous photocatalysis is a surface-based process, because the large surface area can provide more surface active sites for the adsorption of reactant molecules, making the photocatalytic process more efficient.[48−50] Moreover, the porous structure is believed to facilitate the transportation of reactants and products through the interior space due to the interconnected porous network and to favor the harvesting of exciting light due to enlarged surface area and multiple scattering

dx.doi.org/10.1021/nl202587b |*Nano Lett.* 2011, 11, 4774–4779

within the porous framework.[51] Figure 3b shows nitrogen adsorption−desorption isotherms and the corresponding pore size distribution curves of $ZnS(en)_{0.5}$ precursor, CZ0, and CZ2. The nitrogen adsorption−desorption isotherms of all samples are of type IV, indicating the presence of mesopores (2−50 nm). The shape of hysteresis loops is of type H3, associated with aggregates of platelike particles, giving rise to slitlike pores,[52,53] which is well consistent with the scanning electron microscopy (SEM) and TEM results (Figure 1). In addition, the isotherms show high absorption at high relative pressure (P/P_0) range (approaching 1.0), suggesting the formation of large mesopores and macropores.[54] The pore-size distributions (inset in Figure 3b) of the samples indicate a wide pore-size distribution from 2 to 100 nm, further confirming the existence of mesopores and macropores. Supporting Information Table S1 lists the Brunauer−Emmett−Teller (BET) surface areas and pore volumes of the different samples, and the $ZnS(en)_{0.5}$ precursor has the lowest BET surface area and pore volume. After hydrothermal treatment of $ZnS(en)_{0.5}$ precursor with or without Cu^{2+} ions, the CuS/ZnS and pristine ZnS samples exhibit higher BET surface areas and pore volumes than that of $ZnS(en)_{0.5}$ precursor. In addition, the specific surface areas progressively increase with increasing CuS content up to 3%, and then the specific surface areas decrease. It is easy to understand that the BET surface areas and pore volumes of CuS/ZnS samples increase with increasing CuS content at first, because the crystallinity and average crystallite size decrease according to the XRD results. However, higher Cu^{2+} content results in the formation of more CuS nanocrystallites and these nanoparticles may deposit on the surface of ZnS particles or embedded in the pores, thus reducing the specific surface areas and pore volume.

The photocatalytic H_2-production activity of CuS/ZnS porous nanosheets and pristine ZnS (i.e., CZ0) from an aqueous solution containing 0.35 M Na_2S and 0.25 M Na_2SO_3 under visible light irradiation ($\lambda \geq 420$ nm) are compared in Figure 4. Pure ZnS shows a negligible visible light H_2-production activity because the bandgap of ZnS is too large to absorb visible light. In contrast, considerable visible light photocatalytic H_2-production activity is recorded for CuS/ZnS samples. After adding only a small amount of Cu^{2+} in the reaction system, the activity of CZ0.5 is remarkably improved. The photocatalytic activity of the samples increases with increasing the amount of CuS from 0.5 to 2% and reaches a maximum H_2-production rate as high as 4147 μmol h^{-1} g^{-1} with 20% apparent quantum efficiency (QE) at 420 nm for sample CZ2. A further increase in the content of CuS leads to a reduction of the photocatalytic activity. Especially for sample CZ5, the activity for H_2 produciton decreases dramatically. This is probably due to the combined effects of the following several factors: (i) high Cu^{2+} content leads to the deposition of excessive CuS clusters and thus decrease the surface active sites of ZnS; (ii) excessive CuS covered on the surface of ZnS may shield the incident light, and thus prevent the light absorption and generation of photogenerated electrons by ZnS inside; (iii) the increase of their particle size results in deterioration of the catalytic properties of CuS clusters or disappearance of surface effect;[55] (iv) CuS at high content may act as charge recombination centers, resulting in the decrease of the photocatalytic activity. However, sample ZnS + CuS (physical mixture of CuS and ZnS) demonstrates a negligible visible light H_2-production activity. This is ascribed to fact that mechanical mixture of CuS and ZnS is difficult to form close

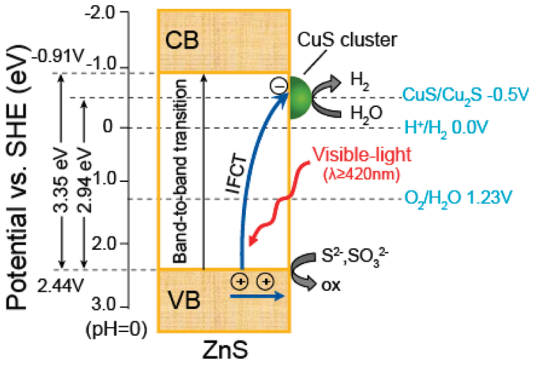

Figure 5. Schematic illustration for visible light induced IFCT from the valence band of ZnS to the CuS clusters in CuS/ZnS system as the proposed mechanism for photocatalytic H_2 production.

interaction (or heterojunction) between the two components and the intimate contact is crucial for the interelectron transfer.[31,32] As a consequence, the direct IFCT could not happen for sample ZnS + CuS, which has been proved by UV−vis results, and thus no visible light activity. Control experiments indicated that no appreciable hydrogen production was detected in the absence of either irradiation or photocatalyst, suggesting that hydrogen was produced by photocatalytic reactions on photocatalyst. In addition, no hydrogen can be detected when CuS alone is used as the catalyst (data not shown here), suggesting that pure CuS is not active for photocatalytic H_2 production under the experimental conditions studied. Interestingly, when using ZnS nanoparticles (NPs) as precursor, the prepared sample CZ2-NPs show much lower H_2-production activity than that of sample CZ2. This result clearly demonstrates that the good photocatalytic activity of CZ2 is associated with the formation of sheetlike porous structures. The sheetlike porous structures are expected to exhibit not only high light-collection efficiency and a fast motion of charge carriers[56,57] but also provide efficient transport pathways to reactant and product molecules,[54] which greatly enhance the photocatalytic H_2-production activity. According to the results reported by our and other groups,[18−26,58] the quantum efficiencies of $Cd_{1-x}Zn_xS$, $ZnS-In_2S_3-Ag_2S$, $Cu-Cd_{1-x}Zn_xS$, $Cu-ZnIn_2S_4$ photocatalysts without noble metals are in the range of 9.6−22.6% at 420 nm. Therefore, the prepared CuS/ZnS porous nanosheets in this work are one of the most highly active metal sulphide photocatalysts in the absence of noble metal cocatalysts. More importantly, only Cu^{2+} ions were used to modify ZnS, instead of harmful cadmium or other expensive elements (such as Ag or In) in the experiment.

From what has been observed and discussed above, several important conclusions can be obtained: (1) Due to the great difference of solubility products (K_{sp}) of ZnS (1.6×10^{-24}) and CuS (6.3×10^{-36}), ZnS could be spontaneously transformed into CuS preferentially on the surface of ZnS particles in the presence of Cu^{2+} (as shown in Figure 1d). (2) Pure ZnS nanosheets are not active for photocatalytic hydrogen generation under visible light irradiation. However, the photocatalytic activity of CuS/ZnS samples can be remarkably improved. (3) By tuning the Cu^{2+} content, the H_2-production activity of CuS/ZnS samples can be controlled. (4) The sheetlike porous structure is believed to greatly enhance the photocatalytic activity. On the basis of the above results, the visible light

dx.doi.org/10.1021/nl202587b |Nano Lett. 2011, 11, 4774–4779

photocatalytic H_2-production mechanism of CuS/ZnS porous nanosheets is proposed as illustrated in Figure 5. First, the bandgap of ZnS is found to be 3.35 eV based on the UV−vis results, then the band edge positions of the CB and VB of ZnS can be determined by the following equation[55]

$$E_{CB} = \chi - E^e - \frac{1}{2}E_g \quad (1)$$

where E_{CB} is the conduction band edge potential, χ is the electronegativity of the semiconductor, expressed as the geometric mean of the absolute electronegativity of the constituent atoms, which is defined as the arithmetic mean of the atomic electron affinity and the first ionization energy. E^e is the energy of free electrons on the hydrogen scale ca. 4.5 eV. E_g is the bandgap of the semiconductor. The calculated conduction and valence band positions of ZnS prepared in our experimental condition at the point of zero are about −0.91 and 2.44 eV, respectively. Obviously, the band-to-band transition of ZnS cannot be excited under visible light irradiation due to the large bandgap energy, and the pure CuS also shows no visible light activity. However, the prepared CuS/ZnS samples show high visible light H_2-production rate, so how could be the visible light H_2-production activity explained? Very recently, Irie and Hashimoto et al. reported that Cu(II)-TiO_2, Cu(II)-WO_3, Cu(II)-$Ti_{1-3x}W_xGa_{2x}O_2$ and Cu(II)-$(Sr_{1-y}Na_y)(Ti_{1-x}Mo_x)O_3$ systems are sensitive to visible light.[44−47] For the above-mentioned systems, they proposed that visible light initiates IFCT as theoretically formulated by Creutz et al.[59] That is, electrons in the VB of semiconductors are transferred directly to Cu(II) under visible light irradiation. We propose that visible light irradiation also induces IFCT from the VB of ZnS to CuS clusters in our work. The direct evidence is the enhanced absorption from ∼350 to 450 nm due to the IFCT from the VB of ZnS to CuS, as shown in Figure 3a, and this charge transfer is shown by the blue bold arrow in Figure 5. The transferred electrons from the VB of ZnS to CuS cause the partial reduction of CuS to Cu_2S, which has been confirmed by the previous XPS results (see Figure 2). Furthermore, the potential of CuS/Cu_2S is about -0.5 V (vs SHE, pH = 0), and the interfacial transition energy from the VB of ZnS to CuS/Cu_2S is determined to be 2.94 eV. Therefore, it is reasonable to assume that the absorption from ∼350 to 450 nm can be ascribed to the direct IFCT from the VB of ZnS to CuS. The transferred photoinduced electrons in CuS clusters from the VB of ZnS could effectively reduce protons to produce H_2 molecules; meanwhile, the holes in the VB of ZnS could be consumed by the sacrificial agents (S^{2-}, SO_3^{2-}). Consequently, this IFCT will retard the recombination of photoinduced electrons and holes due to space separation and lead to hydrogen production. Thus, it is not surprising that when x is lower than 2 with increasing Cu content more CuS clusters are deposited on the surface of ZnS, resulting in the increase of the H_2-production activity because of more IFCT electrons produced. It should be noted that at the beginning, the transferred electrons from the VB of ZnS to CuS clusters will cause the partial reduction of CuS to Cu_2S, forming Cu_2S clusters. These CuS/Cu_2S clusters can work as an electron sink and cocatalyst to promote the separation and transfer of photogenerated electrons from the VB of ZnS to the CuS/Cu_2S cluster, where H^+ is reduced to hydrogen molecules. The major electron transfer steps in the above photocatalytic H_2-production mechanism under visible light irradiation are summarized by the following equations

$$CuS/ZnS + h\nu \rightarrow CuS(e^-)/ZnS(h^+) \quad (2)$$

$$2CuS + 2e^- \rightarrow Cu_2S + S^{2-} \quad (3)$$

$$Cu_2S + 2H^+ + S^{2-} \rightarrow 2CuS + H_2 \quad (4)$$

On the contrary, with further increasing the content of CuS up to higher than 2% excessive CuS clusters will shield the incident light.[60,61] The negative effects of CuS at high concentrations cause the decrease of the photocatalytic H_2-production activity.

In summary, CuS/ZnS porous nanosheets are prepared for the first time via hydrothermal treatment and cation exchange reactions using the preformed $ZnS(en)_{0.5}$ nanosheets and Cu$(NO_3)_2$ as precursors. The prepared CuS/ZnS porous nanosheets show especially high visible light photocatalytic H_2-production activity even without Pt cocatalyst. The content of surface deposited CuS exhibits a significant influence on the visible light photocatalytic H_2-production activity. The optimal CuS loading content is determined to be about 2 mol % and the corresponding H_2-production rate is 4147 μmol h^{-1} g^{-1} with QE of 20% at 420 nm. It is believed that visible light irradiation induces the direct IFCT from the VB of ZnS to CuS, which results in the reduction of CuS to Cu_2S. The potential of CuS/Cu_2S is about −0.5 V (vs SHE, pH = 0), which is more negative than H^+/H_2 potential and favors the reduction of H^+, thus enhancing the photocatalytic H_2-production activity. The interfacial transition energy from the VB of ZnS (2.44 V) to CuS/Cu_2S (−0.5 V) is determined to be ca. 2.94 eV, which thus causes the absorption from ∼350 to 450 nm in the UV−vis diffused reflectance spectra. This work not only shows a possibility for replacing noble metal catalysts by economical CuS in the photocatalytic H_2 production but also for the first time exhibits a facile method for enhancing H_2-production activity by photoinduced IFCT.

■ ASSOCIATED CONTENT

Supporting Information. Additional information about sample preparation, characterization and physicochemical properties, measurements of photocatalytic H_2-prodution activity, SEM, TEM, and XRD. This material is available free of charge via the Internet at http://pubs.acs.org.

■ AUTHOR INFORMATION

Corresponding Author
*E-mail: (J.Y.) jiaguoyu@yahoo.com; (J.R.G.) gongjr@nanoctr.cn.

■ ACKNOWLEDGMENT

This work was partially supported by the National Natural Science Foundation of China (Nos. 20877061, 51072154, 91123003, and 21005023) and the Natural Science Foundation of Hubei Province (2010CDA078). Also, this work was financially supported by the National Basic Research Program of China (Nos. 2011CB933401, 2009CB939704, and 2007CB613302) and Self-determined and Innovative Research Funds of SKLWUT.

REFERENCES

(1) Cortright, R. D.; Davda, R. R.; Dumesic, J. A. *Nature* **2002**, *418*, 964–967.
(2) Turner, J. A. *Science* **2004**, *305*, 972–974.
(3) Fujishima, A.; Honda, K. *Nature* **1972**, *238*, 37–38.
(4) Kudo, A.; Miseki, Y. *Chem. Soc. Rev.* **2009**, *38*, 253–278.
(5) Abe, R.; Higashi, M.; Sayama, K.; Abe, Y.; Sugihara, H. *J. Phys. Chem. B* **2006**, *110*, 2219–2226.
(6) Sato, J.; Saito, N.; Nishiyama, H.; Inoue, Y. *J. Phys. Chem. B* **2001**, *105*, 6061–6063.
(7) Yerga, R. M. N.; Galvan, M. C. A.; del Valle, F.; de la Mano, J. A. V.; Fierro, J. L. G. *ChemSusChem* **2009**, *2*, 471–485.
(8) Li, Q.; Guo, B. D.; Yu, J. G.; Ran, J. R.; Zhang, B. H.; Yan, H. J.; Gong, J. R. *J. Am. Chem. Soc.* **2011**, *133*, 10878–10884.
(9) Hu, J. S.; Ren, L. L.; Guo, Y. G.; Liang, H. P.; Cao, A. M.; Wan, L. J.; Bai, C. L. *Angew. Chem., Int. Ed.* **2005**, *44*, 1269–1273.
(10) Reber, J. F.; Meier, K. *J. Phys. Chem.* **1984**, *88*, 5903–5913.
(11) Youn, H. C.; Baral, S.; Fendler, J. H. *J. Phys. Chem.* **1988**, *92*, 6320–6327.
(12) Kudo, A.; Sekizawa, M. *Chem. Commun.* **2000**, 1371–1372.
(13) Arai, T.; Senda, S. I.; Sato, Y.; Takahashi, H.; Shinoda, K.; Jeyadevan, B.; Tohji, K. *Chem. Mater.* **2008**, *20*, 1997–2000.
(14) Tsuji, I.; Kudo, A. *J. Photochem. Photobiol. A: Chem.* **2003**, *156*, 249–252.
(15) Bang, J. H.; Helmich, R. J.; Suslick, K. S. *Adv. Mater.* **2008**, *20*, 2599–2603.
(16) Lei, Z.; You, W.; Liu, M.; Zhou, G.; Takata, T.; Hara, M.; Domen, K.; Li, C. *Chem. Commun.* **2003**, 2142–2143.
(17) Xing, C. J.; Zhang, Y. J.; Yan, W.; Guo, L. J. *Int. J. Hydrogen Energy* **2006**, *31*, 2018–2024.
(18) Zhang, K.; Jing, D. W.; Xing, C. J.; Guo, L. J. *Int. J. Hydrogen Energy* **2007**, *32*, 4685–4691.
(19) Yu, J. G.; Zhang, J.; Jaroniec, M. *Green Chem.* **2010**, *12*, 1611–1614.
(20) Zhang, W.; Zhong, Z. Y.; Wang, Y. S.; Xu, R. *J. Phys. Chem. C* **2008**, *112*, 17635–17642.
(21) Zhang, W.; Xu, R. *Int. J. Hydrogen Energy* **2009**, *34*, 8495–8503.
(22) Liu, G. J.; Zhao, L.; Ma, L. J.; Guo, L. J. *Catal. Commun.* **2008**, *9*, 126–130.
(23) Shen, S. H.; Zhao, L.; Zhou, Z. H.; Guo, L. J. *J. Phys. Chem. C* **2008**, *112*, 16148–16155.
(24) Li, Y. X.; Chen, G.; Wang, Q.; Wang, X.; Zhou, A. K.; Shen, Z. Y. *Adv. Func. Mater.* **2010**, *20*, 3390–3398.
(25) Kudo, A.; Sekizawa, M. *Catal. Lett.* **1999**, *58*, 241–243.
(26) Ikeda, S.; Nakamura, T.; Harada, T.; Matsumura, M. *Phys. Chem. Chem. Phys.* **2010**, *42*, 13943–13949.
(27) Deng, Z. X.; Wang, C.; Sun, X. M.; Li, Y. D. *Inorg. Chem.* **2002**, *41*, 869–873.
(28) Yu, S. H.; Yoshimura, M. *Adv. Mater.* **2002**, *14*, 296–300.
(29) Ni, Y. H.; Cao, X. F.; Hu, G. Z.; Yang, Z. S.; Wei, X. W.; Chen, Y. H.; Xu, J. *Cryst. Growth Des.* **2007**, *7*, 280–285.
(30) Liu, J. Y.; Guo, Z.; Meng, F. L.; Luo, T.; Li, M. Q.; Liu, J. H. *Nanotechnology* **2009**, *20*, 125501.
(31) Zong, X.; Yan, H. J.; Wu, G. P.; Ma, G. J.; Wen, F. Y.; Wang, L.; Li, C. *J. Am. Chem. Soc.* **2008**, *130*, 7176–7177.
(32) Maeda, K.; Xiong, A. K.; Yoshinaga, T.; Ikeda, T.; Sakamoto, N.; Hisatomi, T.; Takashima, M.; Lu, D. L.; Kanehara, M.; Setoyama, T.; Teranishi, T.; Domen, K. *Angew. Chem., Int. Ed.* **2010**, *49*, 4096–4099.
(33) Shen, S. H.; Guo, L. J.; Chen, X. B.; Ren, F.; Mao, S. S. *Int. J. Hydrogen Energy* **2010**, *35*, 7110–7115.
(34) Yu, J. G.; Wang, G. H.; Cheng, B.; Zhou, M. H. *Appl. Catal., B* **2007**, *69*, 171–180.
(35) Yu, J. G.; Dai, G. P.; Cheng, B. *J. Phys. Chem. C* **2010**, *114*, 19378–19385.
(36) Yu, J. G.; Hai, Y.; Cheng, B. *J. Phys. Chem. C* **2011**, *115*, 4953–4958.
(37) Yu, J. G.; Zhang, J.; Liu, S. W. *J. Phys. Chem. C* **2010**, *114*, 13642–13649.
(38) Ghijsen, J.; Tjeng, L. H.; Elp, J. V.; Eskes, H.; Westerink, J.; Sawatzky, G. A.; Czyzyk, M. T. *Phys. Rev. B* **1988**, *38*, 11322–11330.
(39) *Handbook of X-ray Photoelectron Spectroscopy*; Moulder, J. F., Stickle, W. F., Sobol, P. E., Bomben, K. D., Chastain, J., Eds.; Physical Electronics, Inc.: Eden Prairie, MN, 1992.
(40) Shan, J.; Pulkkinen, P.; Vainio, U.; Maijala, J.; Merta, J.; Jiang, H.; Serimaa, R.; Kauppinen, E.; Tenhu, H. *J. Mater. Chem.* **2008**, *18*, 3200–3208.
(41) Yu, X. X.; Yu, J. G.; Cheng, B.; Huang, B. B. *Chem.—Eur. J.* **2009**, *15*, 6731–6739.
(42) Serpone, N.; Lawless, D.; Khairutdinov, R. *J. Phys. Chem.* **1995**, *99*, 16646–16654.
(43) Zhao, Y. X.; Pan, H. C.; Lou, Y. B.; Qiu, X. F.; Zhu, J. J.; Burda, C. *J. Am. Chem. Soc.* **2009**, *131*, 4253–4261.
(44) Qiu, X. Q.; Miyauchi, M.; Yu, H. G.; Irie, H.; Hashimoto, K. *J. Am. Chem. Soc.* **2010**, *132*, 15259–15267.
(45) Yu, H. G.; Irie, H.; Hashimoto, K. *J. Am. Chem. Soc.* **2010**, *132*, 6898–6899.
(46) Irie, H.; Miura, S.; Kamiya, K.; Hashimoto, K. *Chem. Phys. Lett.* **2008**, *457*, 202–205.
(47) Irie, H.; Kamiya, K.; Shibanuma, T.; Miura, S.; Tryk, D. A.; Yokoyama, T.; Hashimoto, K. *J. Chem. Phys. C* **2009**, *113*, 10761–10766.
(48) Hoffmann, M. R.; Martin, S. T.; Choi, W.; Bahnemann, D. W. *Chem. Rev.* **1995**, *95*, 69–96.
(49) Yu, J. G.; Zhang, L. J.; Cheng, B.; Su, Y. R. *J. Phys. Chem. C* **2007**, *111*, 10582–10589.
(50) Yu, J. G.; Wang, W. G.; Cheng, B. *Chem. Asian J.* **2010**, *5*, 2499–2506.
(51) Yu, J. G.; Yu, J. C.; Leung, M. K.;P.; Ho, W.; Cheng, B.; Zhao, X.; Zhao, J. *J. Catal.* **2003**, *217*, 69–78.
(52) Sing, K. S. W.; Everett, D. H.; Haul, R. A. W.; Moscou, L.; Pierotti, R. A.; Rouquerol, J.; Siemieniewska, T. *Pure Appl. Chem.* **1985**, *57*, 603–619.
(53) Yu, J. G.; Qi, L. F.; Jaroniec, M. *J. Phys. Chem. C* **2010**, *114*, 13118–13125.
(54) Yu, J. G.; Fan, J. J.; Cheng, B. *J. Power Sources* **2011**, *196*, 7891–7898.
(55) Yu, J. G.; Ran, J. R. *Energy Environ. Sci.* **2011**, *4*, 1364–1371.
(56) Yu, J. G.; Fan, J. J.; Lv, K. L. *Nanoscale* **2010**, *2*, 2144–2149.
(57) Xiang, Q. J.; Lv, K. L.; Yu, J. G. *Appl. Catal., B* **2010**, *96*, 557–564.
(58) Li, Y. X.; Chen, G.; Zhou, C.; Sun, J. X. *Chem. Commun.* **2009**, 2020–2022.
(59) Creutz, C.; Brunschwig, B. S.; Sutin, N. *J. Phys. Chem. B* **2006**, *110*, 25181–25190.
(60) Yu, J. G.; Ma, T. T.; Liu, S. W. *Phys. Chem. Chem. Phys.* **2011**, *13*, 3491–3501.
(61) Yu, J. G.; Ma, T. T.; Liu, G.; Cheng, B. *Dalton Trans.* **2011**, *40*, 6635–6644.

Supporting Information

Visible-Light Photocatalytic H_2-Production Activity of CuS/ZnS Porous Nanosheets Based on Photoinduced Interfacial Charge Transfer

Jun Zhang,[†] Jiaguo Yu,[†,*] Yimin Zhang,[†] Qin Li, [‡,†] Jian Ru Gong[‡,*]

[†] State Key Laboratory of Advanced Technology for Materials Synthesis and Processing, College of Resource and Environmental Engineering, Wuhan University of Technology, Wuhan 430070, People's Republic of China

[‡] National Center for Nanoscience and Technology, 11 Zhongguancun Beiyitiao, Beijing 100190, People's Republic of China

*Correspondence: jiaguoyu@yahoo.com, gongjr@nanoctr.cn.

Sample preparation. All the reagents were of analytical grade and were used without further purification. Distilled water was used in all experiments.

Synthesis of $ZnS(en)_{0.5}$ precursor. $ZnS(en)_{0.5}$ nanosheets were prepared by an ethylenediamine assisted solvothermal method according to previous reports.[1-4] In a typical synthesis, 2 mmol $ZnCl_2$ and 4 mmol thiourea were dissolved in 60 mL of ethylenediamine under constant stirring. After stirring for 30 min at room temperature, the mixed solution was then transferred to a 100-mL Teflon-lined

autoclave and maintained at 180 ^{o}C for 18 h. After that, the precipitate was collected by centrifuge, washed with distilled water and ethanol for three times, and then dried in an oven at 60 ^{o}C for 10 h.

Synthesis of ZnS and CuS/ZnS porous nanosheets. ZnS and CuS/ZnS porous nanosheets were synthesized by a hydrothermal and cation exchange method using the above prepared $ZnS(en)_{0.5}$ and $Cu(NO_3)_2$ as precursors. Typically, $ZnS(en)_{0.5}$ nanosheets (0.1 g) were ultrasonically dispersed in water, and then a certain volume of $Cu(NO_3)_2$ aqueous solution (1 mM) was quickly added. The nominal molar ratios of Cu/Zn, which hereafter was designated as *x*, were 0, 0.5, 1, 2, 3 and 5 mol % (see Table S1), and the obtained samples were labeled as CZ0, CZ0.5, CZ1, CZ2, CZ3 and CZ5, respectively. The volume of mixed solution was adjusted to 60 mL with deionized water and stirring for 30 min at room temperature. After that, the suspension was transferred to a 100-mL teflon-lined autoclave and maintained at 140 ^{o}C for 12 h. The final products were respectively rinsed three times with distilled water and ethanol, and dried at 60 ^{o}C for 10 h. According to the previous reports, ZnS could be transformed into CuS completely by cation exchange reactions with excessive Cu^{2+} ions due to the great difference in solubility products (K_{sp}) of ZnS (1.6×10^{-24}) and CuS (6.3×10^{-36}).[5,6] Thus, pure CuS sample was prepared by adding highly excessive Cu^{2+} ions (the molar ratios of Cu/Zn is 50 : 1) in the synthesis procedure. Sample ZnS+CuS was prepared by mechanical mixture of pure CuS and ZnS (i.e. CZ0) with the molar content of CuS equal to 2%. In addition, for comparing, ZnS nanoparticles (NPs) were also prepared using $Zn(NO_3)_2$ and thiourea as raw materials by the hydrothermal method. That is, 2 mmol $Zn(NO_3)_2$ and 4 mmol thiourea were dissolved in 60 mL of distilled water under constant stirring, and then the mixed solutions were transferred to a 100-mL Teflon-lined autoclave and

maintained at 180 ^{o}C for 18 h. CZ2-NPs was also prepared by a hydrothermal and cation exchange method using the above-prepared ZnS nanoparticles and $Cu(NO_3)_2$ as precursors under the above same experimental conditions and the nominal molar ratio of Cu/Zn is equal to 2 mol %.

Characterization. X-ray diffraction (XRD) patterns were obtained on an X-ray diffractometer (type HZG41B-PC) using Cu Kα radiation at a scan rate of 0.05^{o} 2θ s^{-1}. The crystallite size was calculated using Scherrer formula ($d = 0.9\lambda/B\cos\theta$, where d, λ, B and θ are crystallite size, Cu Kα wavelength (0.15418 nm), full width at half maximum intensity (FWHM) in radians and Bragg's diffraction angle, respectively). The chemical compositions of the samples were measured by inductively coupled plasma atomic emission spectrometry (ICP-AES) using an Optima 4300 DV spectrometer (Perkin Elmer). X-ray photoelectron spectroscopy (XPS) measurement was performed in an ultrahigh vacuum VG ESCALAB 210 electron spectrometer equipped with a multi-channel detector. The spectra were excited using Mg Kα (1253.6 eV) radiation (operated at 200 W) of a twin anode in the constant analyser energy mode with a pass energy of 30 eV. All the binding energies were referenced to the C1s peak at 284.8 eV of the surface adventitious carbon. Scanning electron microscopy (SEM) was carried out by an S-4800 field emission SEM (FESEM, Hitachi, Japan). Transmission electron microscopy (TEM) analyses were conducted by a JEM-2010 electron microscope (JEOL, Japan) at an acceleration voltage of 200 kV. The Brunauer-Emmett-Teller (BET) specific surface area (S_{BET}) of the powders was analyzed by nitrogen adsorption in a Micromeritics ASAP 2020 nitrogen adsorption apparatus (USA). A desorption isotherm was used to determine the pore size distribution by the Barret-Joyner-Halender (BJH) method, assuming a cylindrical pore model. UV-vis diffused reflectance spectra of samples were obtained for the

dry-pressed disk samples using a UV-vis spectrotometer (UV2550, Shimadzu, Japan). $BaSO_4$ was used as a reflectance standard in a UV-vis diffuse reflectance experiment.

Photocatalytic activity. The photocatalytic hydrogen evolution experiments were performed in a 100 mL Pyrex flask at ambient temperature and atmospheric pressure, and openings of the flask were sealed with silicone rubber septum. A 350 W xenon arc lamp through a UV-cutoff filter (≤ 420 nm), which was positioned 20 cm away from the reactor, was used as a visible light source to trigger the photocatalytic reaction. The focused intensity on the flask was ca. 180 mW/cm^2. In a typical photocatalytic experiment, 50 mg of catalyst was dispersed by a constant stirring in 80 mL mixed aqueous solution containing 0.35 M Na_2S and 0.25 M Na_2SO_3. Before irradiation, the system was bubbled with nitrogen for 30 min to remove the air inside and ensured the reaction system in an anaerobic condition. A 0.4 mL gas was intermittently sampled through the septum, and hydrogen was analyzed by gas chromatograph (GC-14C, Shimadzu, Japan, TCD, nitrogen as a carrier gas and 5Å molecular sieve column). All glassware was carefully rinsed with distilled water prior to use.

The apparent quantum efficiency (QE) was measured under the same photocatalytic reaction condition. Four low-power 420 nm-LED (3 W) (Shenzhen LAMPLIC Science Co. Ltd. China), which were positioned 1 cm away from the reactor in four different directions, were used as light sources to trigger the photocatalytic reaction. The focused intensity for each 420 nm-LED was ca. 6.0 mW/cm^2. The QE was calculated according to Eq. (S1):

$$\mathrm{QE}\,[\%] = \frac{\text{number of reacted electrons}}{\text{number of incident photons}} \times 100$$
$$= \frac{\text{number of evolved } H_2 \text{ molecules} \times 2}{\text{number of incident photons}} \times 100 \qquad \text{(S1)}$$

Table S1. Experimental conditions for the preparation of the samples and the corresponding physicochemical properties

Samples	*x*	*Cu (mol.%) (ICP-AES)*	*average crystal size of ZnS (nm)*	*pore volume* ($cm^3\ g^{-1}$)	S_{BET} ($m^2\ g^{-1}$)
$ZnS(en)_{0.5}$	-	-	-	0.06	16.6
CZ0	0	0	19.8	0.07	22.0
CZ0.5	0.5	0.38	19.0	0.12	34.5
CZ1	1	0.59	18.3	0.12	36.7
CZ2	2	1.12	17.4	0.13	37.5
CZ3	3	2.03	16.4	0.13	38.9
CZ5	5	3.91	15.7	0.12	35.4

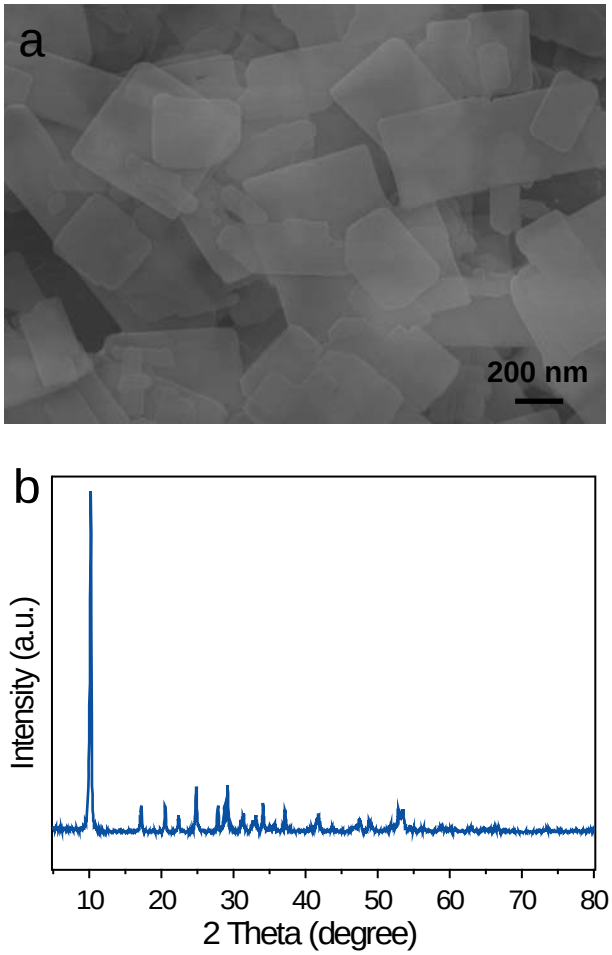

Figure S1. SEM image (a) and corresponding XRD pattern (b) of $ZnS(en)_{0.5}$ precursor.

The typical morphology of the as-prepared $ZnS(en)_{0.5}$ precursor is shown in the SEM image (Figure S1a), exhibiting a sheet-like structure with rectangle lateral dimensions in the range of 0.3-2 μm. The strong and sharp diffraction peaks in the corresponding XRD pattern (Figure S1b) imply good crystallinity and large particle size of the product, which is in good agreement with that of $ZnS(en)_{0.5}$ reported in literatures.[3,4] It was reported that lamellar $ZnS(en)_{0.5}$ compound could be converted into ZnS or ZnO nanosheets under heating conditions in vacuum or in air.[1-4] Nevertheless, a high-temperature heat treatment usually suffers from disadvantages related to high cost and complicated synthetic

procedures. Interestingly, in the present work, hydrothermal method was used instead of high temperature calcinations and pure ZnS porous nanosheets could also be obtained without adding Cu^{2+} ions. As shown in Figure S3, after the hydrothermal treatment of $ZnS(en)_{0.5}$ precursor, the sheet structures of prefabricated $ZnS(en)_{0.5}$ precursor are basically remained and these ZnS porous nanosheets are composed of numerous nanoparticles and the pores are formed between these nanoparticles.

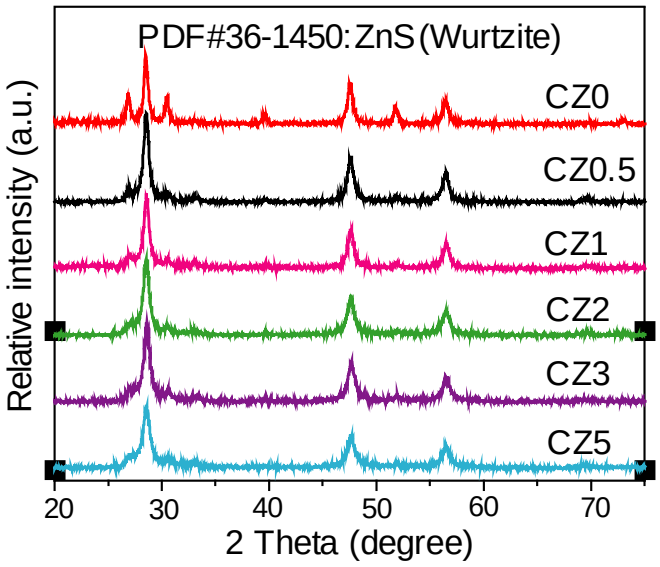

Figure S2. XRD patterns of the CZ***x*** (***x*** = 0, 0.5, 1, 2, 3 and 5 mol %) samples.

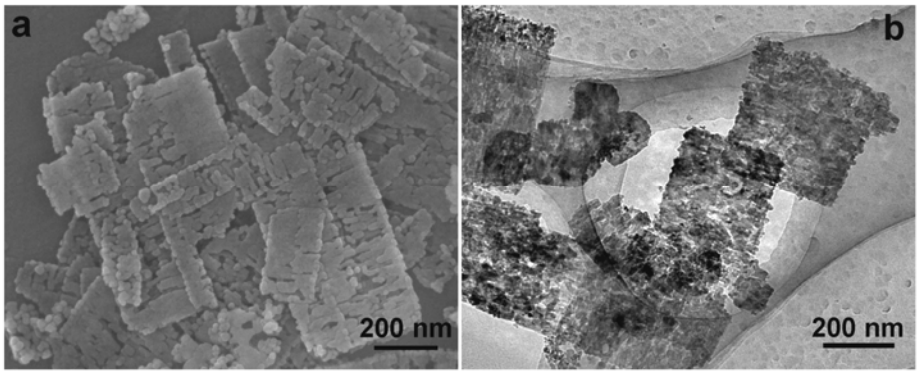

Figure S3. SEM (a) and TEM (b) images of sample CZ0.

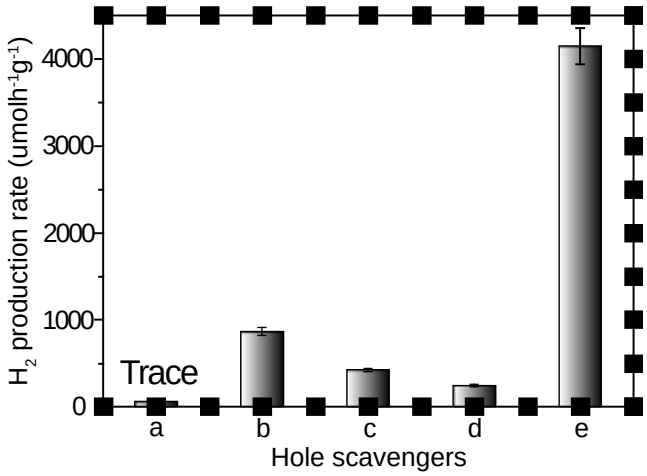

Figure S4. The comparison of photocatalytic H_2-production activity of sample CZ2 under visible-light irradiation ($\lambda \geq 420$ nm) using different hole scavengers: (a) 25%V methanol, (b) 25%V ethanol, (c) 25% glycerol, (d) 25%V lactic acid (e) 0.35 M Na_2S+0.25 M Na_2SO_3

It is well-known that metal sulfide photocatalysts are unstable in the water-oxidation reaction under visible-light because the S^{2-} anions are more susceptible to oxidation than water, thereby causing photocorrosion of the photocatalyst. Furthermore, the common hole scavenger such as methanol and ethanol are excellent fuels themselves.[7] Moreover, as shown in Figure S4, sample CZ2 shows the highest photocatalytic H_2-production activity in the presence of Na_2S/Na_2SO_3 mixture solution as compared with other hole scavengers. Thus, Na_2S/Na_2SO_3 mixture is chosen in this work in order to suppress the photocorrosion of sulfide-based catalysts.

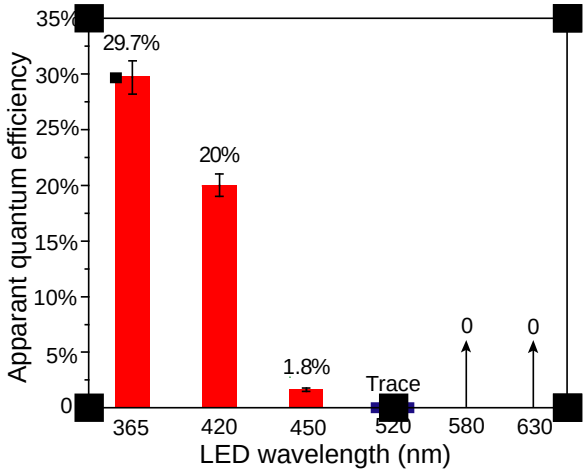

Figure S5. A comparison of apparent quantum efficiency (QE) of sample CZ2 under LED irradiation at different wavelengths using 0.35 M Na_2S and 0.25 M Na_2SO_3 aqueous solution.

The action spectrum is determined by the apparent quantum efficiencies (QE) of the sample CZ2 under LED light irradiation with different wavelength from 365 nm to 630 nm as shown in Figure S5. The potential of Cu^{2+}/Cu^{+} is 0.16 V (vs. SHE, pH=0), however, in this work Cu(II) is existed as CuS and the solubility products (K_{sp}) of CuS is found to be 6.3×10^{-36}. Thus, according to the Nernst equation, the potential of CuS/Cu_2S ($\varphi^{\theta}_{CuS/Cu2S}$) can be calculated as follow:

$$\varphi^{\theta}_{CuS/Cu2S} = \varphi^{\theta}_{Cu2+/Cu+} + 0.059/2\lg([Cu^{2+}]^2/[Cu^{+}]) = \varphi^{\theta}Cu^{2+}/Cu^{+} + 0.059/2\lg(K^{\theta}_{sp}CuS/\ K^{\theta}_{sp}Cu_2S)$$

$$= -0.5\ V$$

The interfacial transition energy from the VB of ZnS to CuS/Cu_2S is determined to be 2.94 eV, thus the maximum excitation wavelength is ca. 420 nm. This result is based on the theory computation; however, such computation is concluded under the standard conditions and also has differences compared with the practical experiments. It should be noted that the other important evidence for the IFCT is absorption

shoulder from 350-450 nm in UV-vis spectra. Thus, the visible-light (≥ 420 nm) can trigger the photocatalytic reactions and the CuS/ZnS samples do show high H_2-production activity under such experimental conditions. As shown in Figure S5, the sample CZ2 shows high H_2-production efficiency at 365 nm and 420 nm, even at 450 nm the sample also exhibits a considerable activity. Furthermore, using the visible-light (≥ 420 nm) is more meaningful for the solar energy utilization and could eliminate the possibility of the intrinsic bandgap absorption of ZnS. Thus, in this work, we choose visible light (≥ 420 nm) to excite the photocatalyst. On the other hand, as shown in Figure 3a, compared with the UV-Vis spectrum of CZ0, the UV-Vis spectrum of CZ2 shows enhanced absorption in the visible-light region (at wavelength over 400 nm), which are attributed to the absorption of CuS and Cu II d-d transitions. However, no hydrogen can be detected when CuS alone is used as the catalyst, suggesting that pure CuS is not active for photocatalytic H_2-production under the experimental conditions studied. Therefore, associated with the action spectrum (Figure S5) the possibility of optical effects contributing to better performance (such as the extra vis-near IR absorption features due to Cu^{2+} d-d transition and CuS itself) could be eliminated.

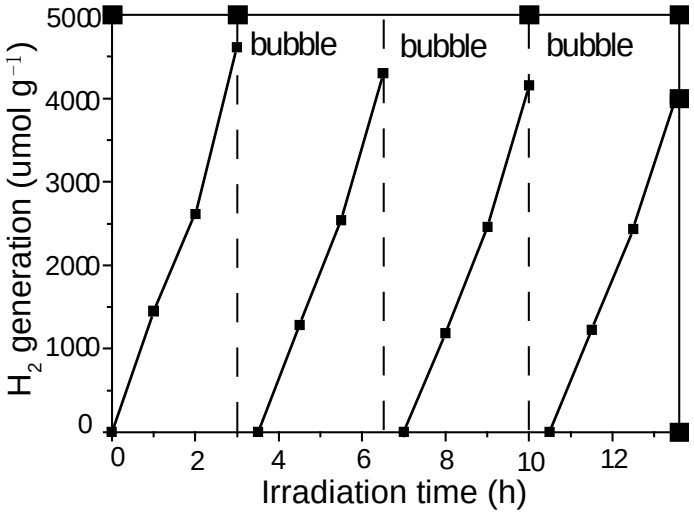

Figure S6. Time course of photocatalytic H_2-production over sample CZ2, every three hours the reaction system is bubbled with N_2 for 30 min to remove the H_2 inside; light source: four low-power 420 nm-LED.

The stability of sample CZ2 was confirmed experimentally by recycling this sample (Figure S6). After four recycles, no significant decrease in the H_2-production rate is observed. The mildly declined in the photocatalytic activity could be due to the consumption of the sacrificial reagents (S^{2-}, SO_3^{2-}), since the concentration of sacrificial reagents affect the performance largely.[8,9] The results indicate that the CuS/ZnS porous nanosheets photocatalysts are highly efficient and stable photocatalysts materials under visible-light irradiation in such experimental conditions.

Cu_2S is just a reaction intermediate in the proposed mechanism. Under visible-light irradiation, the electrons are photoexcitated from VB of ZnS directly to CuS by IFCT and then reduce partial CuS to Cu_2S. CuS nanopatricles could not act as hole scavenger, since the CuS/Cu_2S clusters could act as an electron sink and co-catalyst to reduce H^+ and release H_2. The holes remained in the VB of ZnS could be

consumed by the sacrificial agents (S^{2-}, SO_3^{2-}). Meanwhile, the formed Cu_2S could be oxidized by H^+ and transformed to CuS, because the potential of CuS/Cu_2S (-0.5 V vs. SHE, pH=0) is much more negative than the potential of H^+/H_2 (0 V vs. SHE, pH=0) (as shown in equation 3 and 4). However, the reaction rate of equation 3 is faster than that of equation 4, thus when the photocatalytic reaction was stopped, a small amount of Cu_2S remained in the samples. So, it is not surprising that the XPS results show the presence of Cu^+.

REFERENCES

(1) Deng, Z. X.; Wang, C.; Sun, X. M.; Li, Y. D. *Inorg. Chem.* **2002**, *41*, 869-873.

(2) Yu, S. H.; Yoshimura, M. *Adv. Mater.* **2002**, *14*, 296-300.

(3) Ni, Y. H.; Cao, X. F.; Hu, G. Z.; Yang, Z. S.; Wei, X. W.; Chen, Y. H.; Xu, J. *Crystal Growth & Design*, **2007**, *7*, 280-285.

(4) Liu, J. Y.; Guo, Z.; Meng, F. L.; Luo, T.; Li, M. Q.; Liu, J. H. *Nanotechnology* **2009**, *20*, 125501.

(5) Dloczik, L.; Konenkamp, R. *Nano Lett*. **2003**, *3*, 651-653.

(6) Zhu, Y. F.; Fan, D. H.; Shen, W. Z. *Langmuir* **2008**, *24*, 11131-11136.

(7) Zhang, J.; Liu, S. W.; Yu, J. G.; Jaroniec, M. *J. Mater. Chem.* **2011**, DOI: 10.1039/C1JM12596F

(8) Zhang, W.; Zhong, Z. Y.; Wang, Y. S.; Xu, R. *J. Phys. Chem. C* **2008**, *112*, 17635-17642.

(9) Li, Y. X.; Chen, G.; Wang, Q.; Wang, X.; Zhou, A. K.; Shen, Z. Y. *Adv. Func. Mater.* **2010**, *20*, 3390-3398.